

## Winter Storms over the San Juan Mountains. Part II: Microphysical Processes<sup>1</sup>

WILLIAM A. COOPER AND CLIVE P. R. SAUNDERS<sup>2</sup>

*University of Wyoming, Laramie 82071*

(Manuscript received 13 February 1979, in final form 16 January 1980)

### ABSTRACT

Airborne observations of wintertime storms in southeastern Colorado have shown that the microphysical structure of those storms evolved in close relationship to the dynamical structure. The storms evolved from deep synoptic-scale systems to shallower orographic systems, and in the course of this evolution became unstable. During early storm stages the precipitation developed primarily by diffusional growth of ice crystals, but during later storm stages accretional growth was at least as important as diffusional growth. Early storm stages were almost completely glaciated, but extensive regions of supercooled water appeared in later storm stages. Weak embedded convection also produced important regions of supercooled water in the later storm stages. Ice crystal concentrations were high, often in excess of  $50 \text{ L}^{-1}$ . The observed ice crystal concentrations were far above the corresponding ice nucleus measurements, and the discrepancy could not be attributed to known ice multiplication processes.

### 1. Introduction

In association with the Colorado River Basin Pilot Project (CRBPP), the University of Wyoming studied eight storms during the winter of 1974–75. These storms produced ~25% of the precipitation that fell on experimental days during that winter. As described in Part I of this series (Marwitz, 1980), seven of these storms exhibited the same basic structure. The storms were initially stable systems, then developed instability in the later storm stages. The dynamical and microphysical character of each of these seven storms underwent a consistent evolution, and this consistency of structure has encouraged us to suggest generalized characteristics of wintertime storms of this region.

Part I of this series discussed the airflow and the storm structure. This paper (Part II) presents the microphysical observations in different storm stages. Part III (Cooper and Marwitz, 1980) will assess the seeding potential of these storms and will present an interpretation of the results of the statistical experiment.

The microphysical observations reported in this paper are discussed in greater detail in a project report.<sup>3</sup>

<sup>1</sup> This research was sponsored by the Division of Atmospheric Water Resources Management (now called the Office of Atmospheric Resources Management), Bureau of Reclamation, U.S. Department of the Interior, under Contract 14-06-D-6801.

<sup>2</sup> Present affiliation: Physics Department, UMIST, Sackville Street, Manchester M60 1QD, England.

<sup>3</sup> Marwitz, J. D., W. A. Cooper and C. P. R. Saunders, 1976: Structure and seedability of San Juan storms. Final Report to the Bureau of Reclamation, Denver, CO, 326 pp.

### 2. Data acquisition

#### *a. Ice crystal observations*

Because the detection of ice crystals was of paramount importance to this study, the ice crystal concentrations were measured by three different instruments. Used together, they provided redundant measurements and supplemented each other. A PMS 2D (two-dimensional) probe (described in Knollenberg)<sup>4</sup> provided a continuous record of particle sizes, shapes and concentrations. A Turner-Radke probe (copied after the instrument described in Turner and Radke, 1973) provided a continuous record of ice crystal concentrations and provided ice-water discrimination. In addition, samples of the ice crystals were collected on oil-coated slides exposed in a decelerator. This tapered decelerator, mounted on the side of the aircraft, produced a deceleration ratio of about 11:1, or a typical impact velocity of  $7 \text{ m s}^{-1}$ . The crystals were preserved in chilled hexane until they could be photographed under a microscope. These samples provided valuable information regarding crystal habits and degree of riming, and were also used to check the concentrations, habits and sizes determined from the other ice-detecting instruments.

Table 1 presents a comparison of results from these ice detectors, for a set of 12 oil-coated slide (OCS) samples. Only crystals with maximum dimen-

<sup>4</sup> Knollenberg, R. G., 1976: Three new instruments for cloud physics measurements: The 2-D spectrometer, the forward scattering spectrometer probe, and the active scattering aerosol spectrometer. *Preprints Int. Conf. Cloud Physics*, Boulder, Amer. Meteor. Soc., 554–561.

TABLE 1. Comparison of ice crystal concentrations detected by the 2D probe, the oil-coated slide samples and the Turner-Radke counter.

Date	Slide	Slide concentration (L <sup>-1</sup> )	2D concentration (L <sup>-1</sup> )	Turner-Radke concentration (L <sup>-1</sup> )
29 Dec 74	1	91	82	16
29 Dec 74	2	21	37	3
29 Dec 74	3	8	9	1.5
29 Jan 75	1	7	11	1
29 Jan 75	2	12	7	1
29 Jan 75	3	11	39	3
29 Jan 75	4	25	56	3
30 Jan 75	1	5	12	2
30 Jan 75	2	15	31	5
30 Jan 75	3	20	13	4
21 Mar 75	1	14	17	0.5
21 Mar 75	2	29	56	11

sions  $\geq 50 \mu\text{m}$  were included in OCS and 2D samples. The ratios of concentrations (determined by regression) were  $0.85 \pm 0.19$  (2D:OCS), and  $0.18 \pm 0.03$  (Turner-Radke:OCS) and  $0.84$  (Turner-Radke:2D). The lower ratio between the OCS samples and the Turner-Radke probe is mostly due to the neglect of the detection efficiency of that probe. Turner *et al.* (1976) found the detection efficiency to be  $\sim 35\%$  for  $100 \mu\text{m}$  hexagonal plate crystals. When the concentrations from the Turner-Radke probe were corrected for the detection efficiency of that probe [using the size distributions determined from the oil-coated slides and using the size-dependent efficiencies measured by Turner *et al.*, (1976)], the ratio of concentrations (Turner-Radke:OCS) was  $\sim 0.5$ .

The above comparisons indicate that, for crystal sizes  $\geq 50 \mu\text{m}$ , the measurements of ice crystal concentrations were consistent. These comparisons also indicate that the 2D images were not plagued by "artifacts," such as the streaming of liquid water from the upstream edges of the aperture through the sample volume. These artifacts, which are often a serious problem, are most pronounced in situations where high liquid water is present. For most of these studies only low liquid water contents were present, and careful examination of the 2D images for regions of interest verified that most of the particles detected were true ice particles.

#### b. Liquid water measurements

Three systems were available for the detection of supercooled cloud water. An axially scattering spectrometer probe (ASSP), described by Knollenberg,<sup>4</sup> provided continuous measurements of the cloud droplet concentration and of the size spectrum for droplet diameters from 2 to  $30 \mu\text{m}$ . Liquid water contents were obtained by calculation from

these spectra, and also by independent continuous measurements from a Johnson-Williams hot-wire instrument. The droplet spectra were also measured at selected times by a cloud gun sampler, which obtained accurately timed exposures of soot-coated impactor slides.

Our version of the ASSP was checked extensively during the course of this research. The calibrations (using droplets generated by a monodisperse droplet generator) showed that the ASSP apparently undersized large droplets significantly, but was quite accurate for drop diameters  $< 12 \mu\text{m}$ . For diameters as large as  $30 \mu\text{m}$ , the sizes determined by the ASSP were only about 70% of the true droplet size. The resolution of the probe was  $< 3 \mu\text{m}$  (standard deviation) for droplet diameters  $< 12 \mu\text{m}$ , but increased to  $\sim 5 \mu\text{m}$  for diameters near  $30 \mu\text{m}$ .

In regions where the liquid water content was greater than  $0.1 \text{ g m}^{-3}$ , the water contents determined from the ASSP and from the Johnson-Williams instrument were in about  $\pm 50\%$  agreement. The liquid water contents determined from the cloud-gun slides varied from one to two times the corresponding water contents determined from the ASSP. Because of the variations and inconsistencies in these ratios, we do not trust any of the measurements of liquid water content an accuracy better than about  $\pm 50\%$  of the indicated value. Nevertheless, for this research the instruments provided crucial information regarding the presence or absence of significant quantities of supercooled water. In this regard, all three instruments were consistent.

Recorded observations of the degree of airframe icing were also used to confirm the presence of supercooled liquid water in these storms. The times at which noticeable icing occurred, as recorded in voice notes, corresponded well with the instrumentally determined presence of liquid water in the clouds. Even liquid water contents as low as  $0.1 \text{ g m}^{-3}$  produced noticeable airframe icing.

#### c. Ice nucleus measurements

A rotating filter sampler collected time-resolved filter samples. This sampler has been discussed in Dye *et al.* (1976). The filters were processed (by G. Langer) according to the flow or "puff" technique described in Langer and Rodgers (1975). Previous tests by Dye *et al.* (1976) have shown this to be an effective detection scheme for AgI plumes.

Ice nucleus samples were collected both in and out of cloud. The concentrations obtained in cloud should not be interpreted as quantitative ice nucleus measurements, since much of the seeding material would be in cloud or ice particles. A sample of the cloud, including water and ice, was drawn through the filters. The air warmed sufficiently

while passing through the cabin of the aircraft so that the cloud water evaporated before reaching the filters. Thus, the sample consisted of the particles in the air and all the residue left when the droplets evaporated. If the droplets contained AgI, either in dissolved or particulate form, this AgI would be collected on the filters.

Comparisons between expected and observed seeding signatures will be discussed in Part III. Those comparisons, and the results of Dye *et al.* (1976), support that this is an effective means of detecting AgI plumes in cloud.

#### d. Additional aircraft instrumentation

The aircraft used in this research was a Beechcraft Queen Air (B-80). It was equipped with a data-acquisition and display system featuring real-time display, in engineering units, of both direct measurements and derived parameters. Data were recorded on computer-compatible magnetic tape at 1 s intervals. The standard measurements included temperature (a Rosemount and a reverse-flow probe), dew point (Cambridge system, Peltier-cooled mirror), pressure, airspeed, heading and position (VOR-DME). A Doppler radar and a yaw vane provided measurements from which the horizontal wind could be deduced, and the vertical wind was estimated through the use of a calibration of the expected rate-of-climb as a function of power setting and indicated airspeed. An MRI turbulence meter provided a measurement of the turbulent energy in the wavelengths from 2 to 50 m. Recorded voice notes and event markers were used by all crew members.

#### e. Ground observations

Ground observations (collected and furnished to us by L. Vardiman of the U.S. Bureau of Reclamation) were used to complement the airborne measurements. Samples of the falling snow were col-

lected in cold hexane and photographed under a microscope. Crystal habits and the degree of riming or aggregation of the ice crystals could be determined from these collections. They proved of great value in linking the aircraft observations to surface snowfall.

### 3. Case studies

Case studies were constructed for each of the storms, and are presented in detail in Marwitz *et al.*<sup>3</sup> The following sections present illustrative studies for different storm stages.

#### a. The stable storm stage

The storms normally began as stable systems. Although the initial clouds were often cirrus, the storms rapidly deepened and normally were 3–5 km in depth by the time precipitation began. (See Part I for a full description of the storm evolution.) An example of an early storm stage was studied on 30 January 1975. The flight began as the cloud layer was deepening and as precipitation was starting. The sounding, constructed from aircraft measurements upwind of the mountain barrier, is shown in Fig. 1. The hodograph shows the "blocked flow" pattern characteristic of the stable storm stage. The low-level winds (below 3 km MSL) were weak and from an easterly or southerly direction, so below that altitude the air formed a relatively stagnant air mass which did not flow against the mountain barrier. As a result, the low-level convective instability of Fig. 1 was not released and the storm developed as a stable system. Another result of the blocked airflow was that the upward motions caused by the mountain barrier were small; only the airflow above ~3 km MSL was flowing over the mountain range, and this air was lifted only by the protrusion of the (3.5–4.0 km MSL) mountain barrier above the blocked layer. The resulting vertical deflection of the airflow was much smaller

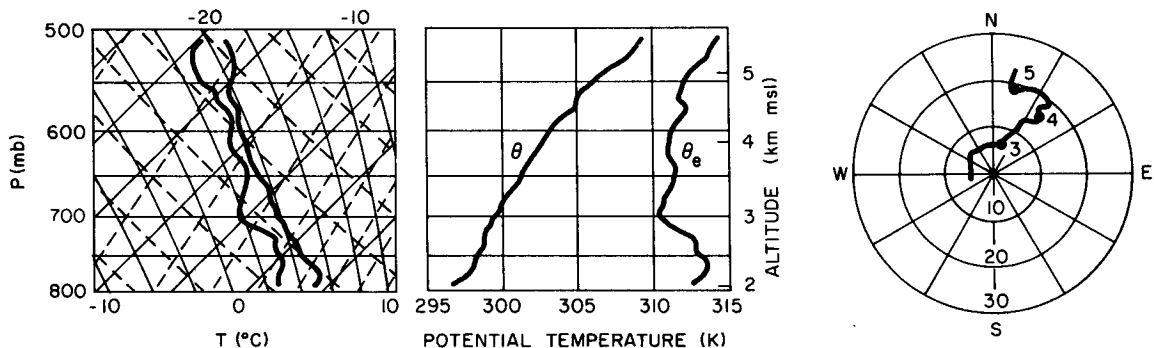


FIG. 1. The sounding measured upwind of the mountain range during the flight of 30 January 1975. Left: temperature and dew point plotted on a skew  $T$  diagram; center: potential temperature ( $\theta_e$ ); right: wind hodograph, with wind magnitude in  $\text{m s}^{-1}$  and with the 3, 4 and 5 km MSL winds labeled.

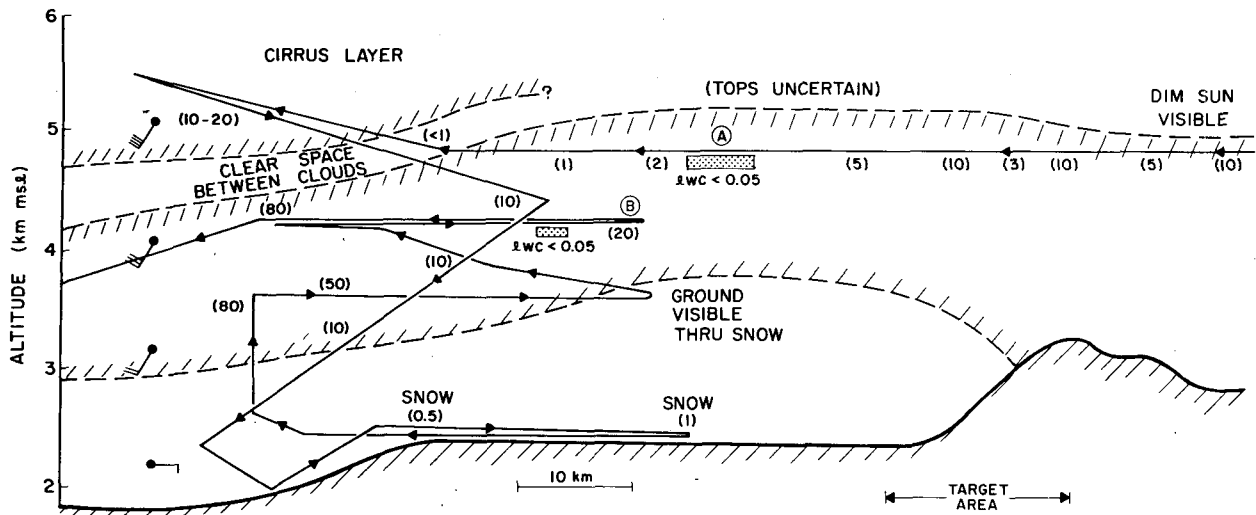


FIG. 2. Vertical cross section for the storm of 30 January 1975. The solid line with arrows shows the flight track, and the dashed lines show cloud boundaries. The numbers in parentheses are representative ice crystal concentrations ( $L^{-1}$ ). The temperature at 4.7 km was  $-15^{\circ}C$ , and at 4.2 km it was  $-12^{\circ}C$ . Regions where supercooled cloud water was detected are indicated by shading. The airflow was from the southwest, or from the left in the figure. The approximate topographic outline is shown by the solid line along the bottom of the figure.

than would have resulted if the entire layer down to the surface were to flow over the barrier.

Fig. 2 shows a vertical cross section of the storm at the time of the flight. The figure shows the flight track and some representative ice crystal concentrations. Evidence that this was a stable cloud system comes from the smooth character of the airflow and from the absence of rapid fluctuations in state parameters or cloud characteristics. Weak gravity waves were characteristic of the stable storm stages, and were reflected in this case by periodic, correlated fluctuations in equivalent potential temperature ( $\theta_e$ ), ice crystal concentration, and ice crystal habit during the level flight segment at 4.8 km altitude. During that flight segment, the value of  $\theta_e$  remained within 1 K of 312.5 K, even over the mountains, indicating the absence of substantial lifting of air over the mountain range.

The seeding generators had been operated during a preceding storm, and were shut down  $\sim 3.5$  h before the start of this flight. In such a blocked flow, the seeding material might have remained in the area upwind of the mountains. However, there was no convective transport, so vertical diffusion would be the only means by which the AgI could reach cloud level. The rotating filter samples did not indicate the presence of AgI at cloud level; concentrations active at  $-19^{\circ}C$  were only the general  $0.1 L^{-1}$  background concentration. The high ice crystal concentrations appeared far upwind of any seeding generators and at high altitudes, as indicated in Fig. 2. The high ice concentrations were present all the way to Farmington, more than 100 km upwind of the seeding generators. These high ice

crystal concentrations could not have been produced by seeding.

Early in the flight, there was a separate cirrus layer above the main storm cloud. This cirrus layer merged with the lower layer as the storm deepened, and as a result much higher ice crystal concentrations were present during the last part of the flight. The concentrations in excess of  $50 L^{-1}$  were composed of a mixture of capped columns, bullets, side plane crystals, and other habits indicating an origin colder than  $-20^{\circ}C$ . These crystals were observed at temperatures as warm as  $-8^{\circ}C$ . Fig. 3 shows some ice crystals collected at point B of Fig. 2, at a temperature of  $-12^{\circ}C$ ; the habits indicate that they originated much higher in the storm.

Near the point marked A in Fig. 2, a very thin supercooled water cloud was detected. The liquid water region only had a liquid water content of  $\sim 0.02-0.03 g m^{-3}$ . The droplet spectrum modal diameter was  $10 \mu m$ , and the total droplet concentration was only  $\sim 50 cm^{-3}$ . This low liquid water content, associated with ice crystal concentrations of only  $\sim 1 L^{-1}$  was the highest liquid water content observed in this cloud.

The absence of supercooled water was reflected in the absence of rime on the crystals collected during this flight. Only one of the ten ice crystal samples showed even light rime on the ice crystals.

The ice crystals collected at the surface in the target area consisted primarily of unrimed or lightly rimed aggregates. The crystal habits were similar to those observed at 4.8 km in the storm. Although some light rime was present, all of the crystals col-

lected were easily recognizable; most of the mass in the precipitation resulted from vapor growth of the ice crystals. The lightly rimed crystals observed near the region A of Fig. 2 apparently fell to the mountain as precipitation. (They would have fallen about 1.5 km while travelling 40 km in  $15 \text{ m s}^{-1}$  average winds, a requirement consistent with a fallspeed of  $50 \text{ cm s}^{-1}$ .)

About an hour after this flight ended, the surface crystal collections consisted of heavily rimed crystals. Three hours after the flight, the crystals were so heavily rimed as to be unrecognizable. These times coincided with the onset of instability in the storm, and with the end of the stable storm stage.

In this instance snowfall during the early stage of the storm was light. During this flight the snowfall at the surface was only  $\sim 1 \text{ mm h}^{-1}$  (melted equivalent). Other stable storm stages had significantly

higher precipitation rates, associated with significantly deeper storm systems.

Two other stable storm stages were studied, and exhibited similar characteristics.

#### *b. The neutral storm stage*

The second stage in the normal storm sequence was a stage in which the lowest layers became neutrally stratified. The "blocked flow" pattern in the low levels ended with the onset of this storm stage, and a surface horizontal convergence zone developed upwind of the mountain barrier. The lifting caused by the mountains was greater than in the stable case, and as a result the neutral case generally had more supercooled water than the stable case. During the neutral stage the cloud tops began to lower, resulting in slightly lower ice crystal concentrations in the storm.

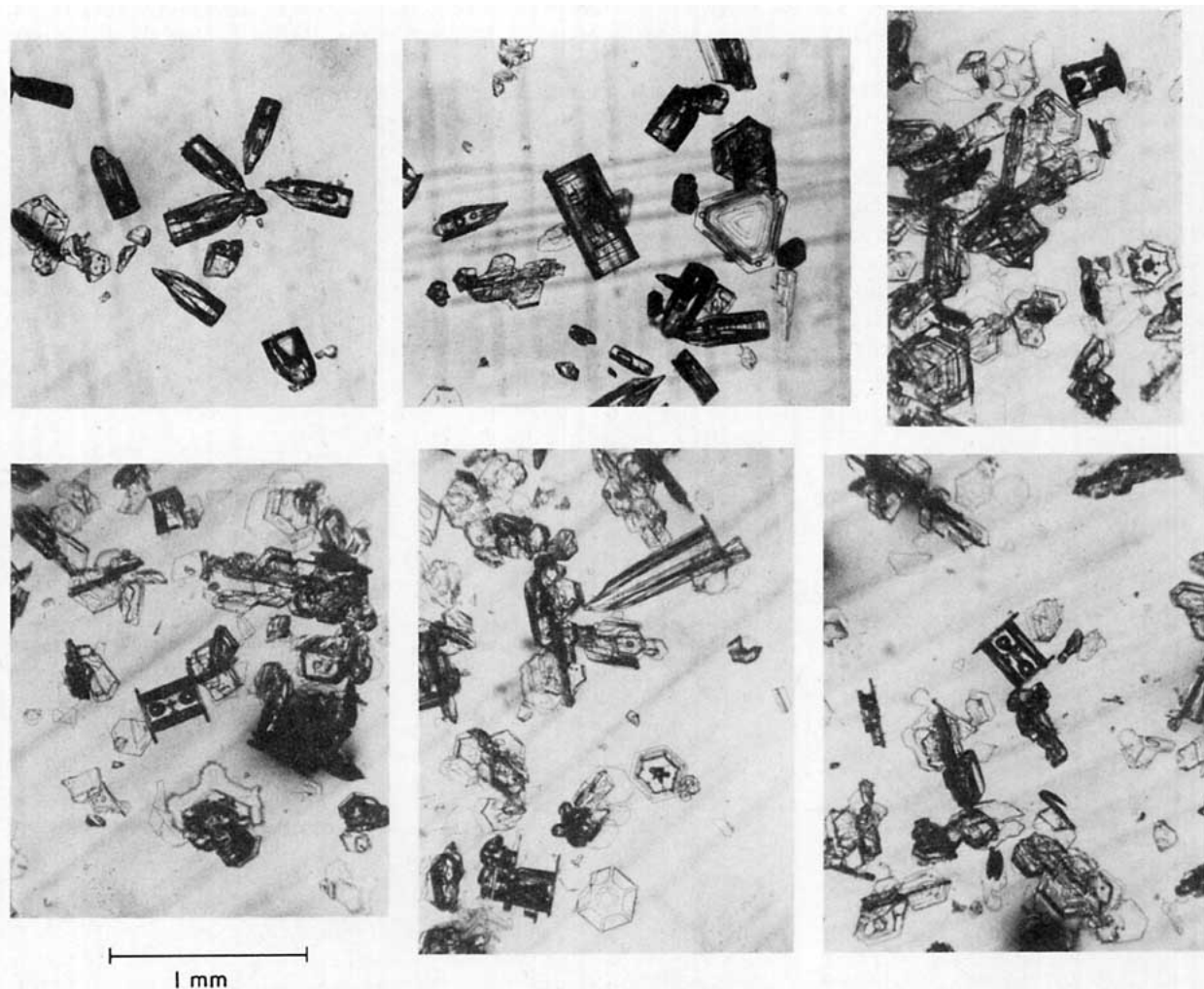


FIG. 3. Examples of ice crystals collected on decelerator slides during the 30 January 1975 flight. The crystals were collected near point B of Fig. 2.

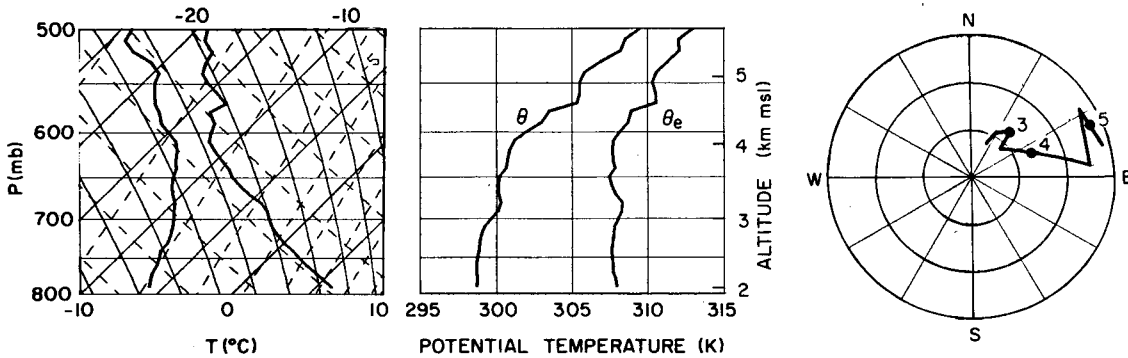


FIG. 4. The sounding measured upwind of the mountains during the flight of 22 March 1975. Left: temperature and dew point, plotted on a skew  $T$  diagram; center: potential and equivalent potential temperatures; right: wind hodograph, with the 3, 4, 5 km MSL winds labeled. Circles correspond to intervals of  $10 \text{ m s}^{-1}$ .

An example of a neutral storm stage was studied on 22 March 1975. The sounding, upwind of the mountains, is shown in Fig. 4. Below cloud base the atmospheric stratification was neutral but above cloud base the layer remained stable. Convection was not present during this stage of the storm. Strong gravity wave patterns were dominant features in the higher levels of the cloud, and have been discussed in Part I.

Fig. 5 shows the vertical section constructed from the aircraft measurements. There were extensive regions where supercooled water was present, but the liquid water contents of the storm seldom exceeded  $0.3 \text{ g m}^{-3}$ . The smooth flow into the upwind portion of this cloud produced a relatively homogeneous region at A in Fig. 5. Strong waves were found at B, with associated fluctuations in

liquid water content and in state parameters. It was normal to find the highest liquid water contents in the region over the mountains, indicated by C. Liquid water contents of  $0.3\text{--}0.4 \text{ g m}^{-3}$  were present in this region of the cloud. The traces of liquid water content and other state parameters indicated that the region C was quite uniform and not affected by convection.

Snowfall rates of  $2\text{--}3 \text{ mm h}^{-1}$  (melted equivalent) fell during the time of this flight. Seeding material was released from the generators until about 3 h before this case study, and the rotating filters did show evidence of low concentrations ( $\sim 1 \text{ L}^{-1}$  active at  $-19^\circ\text{C}$ ) of seeding material in the region C. No AgI was detected at A, as expected in the wind field of Fig. 4. The region of high ice nucleus concentration did not coincide with the

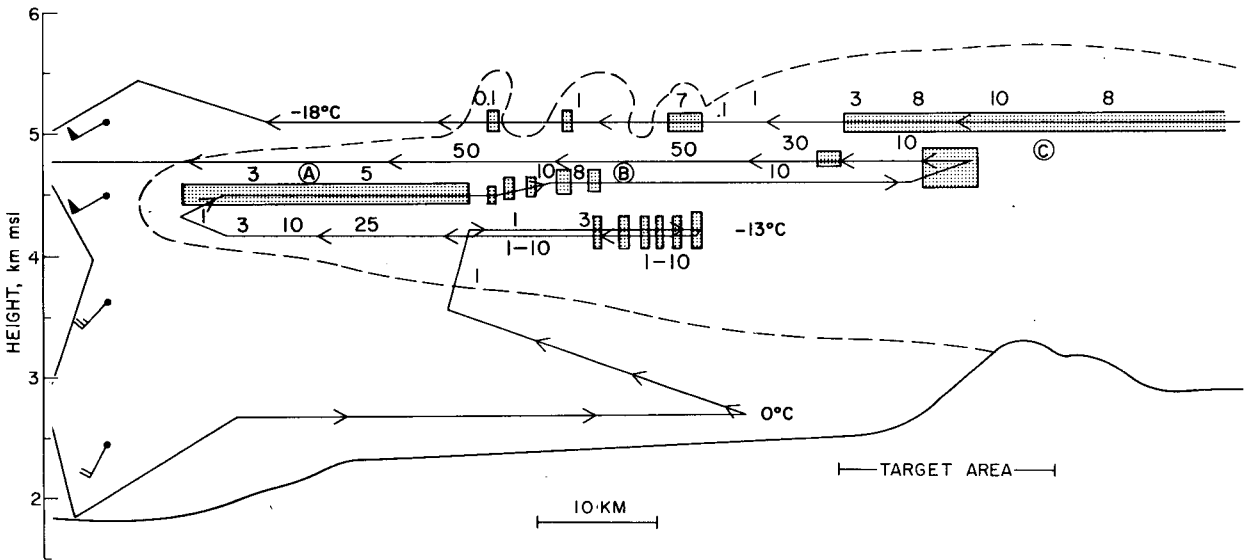


FIG. 5. Vertical cross section for the storm of 22 March 1975. The solid line with arrows indicates the flight track. The dashed line is the outline of the visual cloud. Regions where liquid water contents of  $\geq 0.1 \text{ g m}^{-3}$  were found are shaded, and the numbers along the flight track give representative ice crystal concentrations ( $\text{L}^{-1}$ ). The 0,  $-13$  and  $-18^\circ\text{C}$  levels are indicated; and some regions discussed in the text are denoted by letters. The airflow was from the southwest, or from the left in the figure.

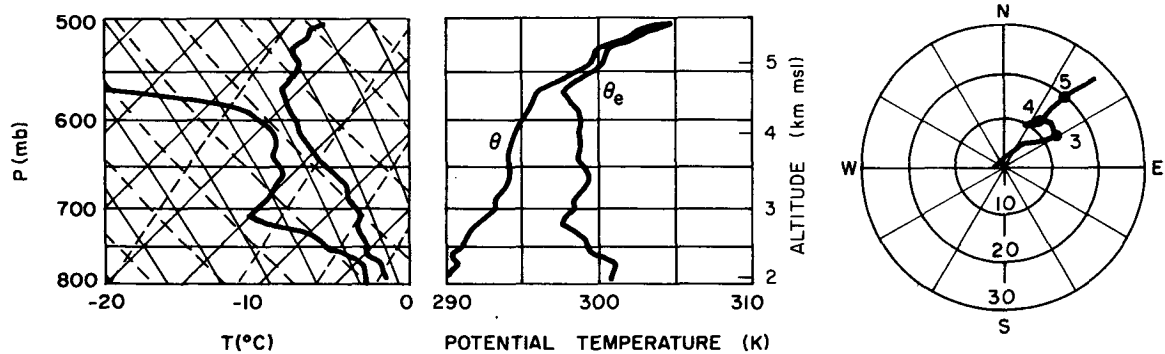


FIG. 6. The sounding measured upwind of the mountains during the flight of 29 December 1974. Left: temperature and dew point, plotted on a skew  $T$  diagram; center: potential and equivalent potential temperatures; right: wind hodograph, with wind magnitudes in  $\text{m s}^{-1}$  and with the 3, 4 and 5 km MSL winds labeled.

region of high ice crystal concentration. High ice concentrations formed well ahead of the mountains, in the layer of clouds beginning at A in Fig. 5, from which the ice could be carried to the region B. However, the high nucleus counts were not detected until C. The evidence seems to indicate that the  $1\text{--}10 \text{ L}^{-1}$  concentrations present at low levels in the storm formed naturally and fell from higher storm regions. Similarly high ice crystal concentrations were also found  $\sim 100 \text{ km}$  upwind of the seeding generators.

### c. The unstable storm stage

As the storm matured, additional destabilization due to upper level cold air advection led to the development of embedded convection within the storm. This convection was symbiotically associated with the horizontal convergence zone located  $\sim 15\text{--}30 \text{ km}$  upwind of the mountains. During the transition from the neutral to the unstable storm stage, the cloud tops normally lowered. Although the atmosphere at high levels cooled during the unstable storm stage, the cloud tops generally became both lower and warmer than in earlier storm stages. The unstable stage often produced heavy precipitation rates.

An example of an unstable storm stage was studied on 29 December 1974. This storm developed in the normal sequence, as discussed in Part I (Marwitz, 1980). The storm was studied in its unstable stage when precipitation rates were  $\sim 2 \text{ mm h}^{-1}$  (melted equivalent). The ground-based seeding generators were operated during the preceding night, but were turned off  $\sim 4\text{--}5 \text{ h}$  before the start of this flight. Because a blocked flow pattern had been present from the preceding night until shortly before the start of this flight, the seeding material was probably present at low levels. In the region directly over the mountains, the rotating filter samples indicated the presence of seeding material

in concentrations about an order of magnitude above the background concentrations. However, only background concentrations of ice nuclei were found in the portions of the storm upwind of the mountains.

Fig. 6 shows the sounding taken upwind of the mountain range. The convective instability in the layer between 2 and 3 km MSL resulted in embedded convection as the air rose over the orographic barrier. Although the cloud was capped by a stable layer and appeared to have a smooth outline, the convective nature of the cloud was apparent in the variations of measured parameters.

Fig. 7 presents some of the aircraft measurements. There were three general regions where supercooled water was present in this storm. These were also regions where liquid water, when present, was found in the other case studies. They were as follows:

(i) Near the upwind cloud edge, and near the rise in topography  $\sim 60 \text{ km}$  upwind of the mountains. A low liquid water content ( $< 0.1 \text{ g m}^{-3}$ ) was observed near the upwind cloud edge at  $-19^\circ\text{C}$ , and another liquid water region was located lower in the cloud near this location. The initial rise in the topography often caused the initial edge of the cloud to form at this location. This particular feature of the topography appeared to be quite influential in determining the storm characteristics. The initial development of cloud far upwind of the mountain range allowed time for ice crystals formed at high altitude to fall to warm regions of the cloud. If the initial rise in the topography had not been present, the upwind edge of the clouds might have been much closer to the mountains and the crystals would not have been able to fall from cold regions of the cloud into the warmer regions.

(ii) Associated with convection  $\sim 15 \text{ km}$  upwind of the target area. This zone (A in Fig. 7) was only pronounced during the unstable storm stages.

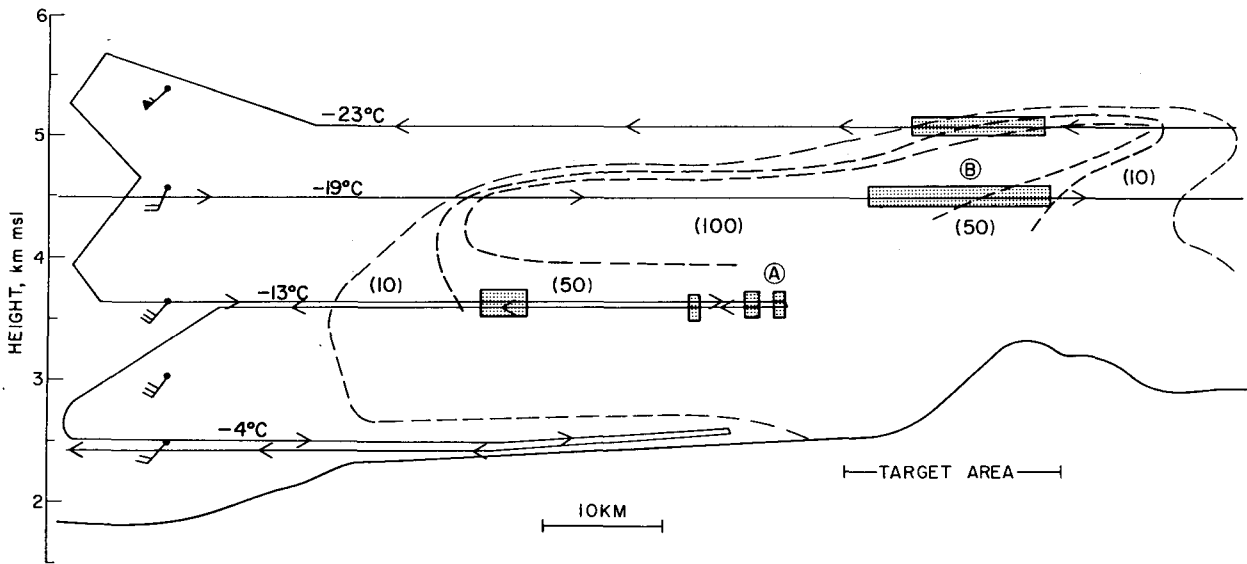


FIG. 7. Vertical cross section for the storm of 29 December 1974. The solid line with arrows shows the flight track, and the dashed lines are approximate contours of the ice crystal concentrations (labeled by the numbers in parentheses, in units of  $L^{-1}$ ). The shaded regions indicate measured liquid water contents in excess of  $0.1 \text{ g m}^{-3}$ . Some representative temperatures are also given, and some regions discussed in the text are denoted by letters. The airflow was from the southwest, or from the left in the figure.

(iii) Ahead of and over the summit. The highest liquid water contents were found in region B of Fig. 7 and were associated with the updrafts due to the mountain range. In this storm the liquid water content in the region over the mountains was  $>0.5 \text{ g m}^{-3}$  through much of region B, and peak values  $> 1.0 \text{ g m}^{-3}$  were observed. This region also contained the largest droplets.

The initial penetration into the upwind edge of this cloud was at  $-19^\circ\text{C}$ . The flow was smooth, with low turbulence values and with no sign of convection. The cloud encountered at the upwind edge, at a temperature of  $-19^\circ\text{C}$ , was ice-free. The liquid water content was very low, and the cloud droplet spectrum typified a newly formed cloud. No ice crystals were detected ahead of the upwind edge of the cloud or  $0.1 \text{ km}$  downwind of the cloud edge. However, within  $2\text{--}3 \text{ km}$  downwind of the edge, ice crystal concentrations of near  $100 \text{ L}^{-1}$  developed, and the liquid water was rapidly depleted. Thereafter, the ice crystal concentration at the  $-19^\circ\text{C}$  level did not change appreciably. This behavior was very similar to that observed in the Elk Mountain cap cloud, discussed in Cooper and Vali<sup>5</sup>.

The crystals observed near the upwind edge of the cloud, at  $-19^\circ\text{C}$ , were plates. Most appeared to be  $\text{Pl}_a$  or  $\text{Cl}_g$  crystals [according to the Magono and Lee (1966) classification]. There was light rime on some

of the crystals, but most had no rime. Clear examples of aggregates were seen in the 2D probe images.

During a flight segment above this cloud, no ice crystals falling from higher levels were found. The system was capped by a layer with  $>10^\circ\text{C}$  dew-point depression. These observations indicate that the observed high ice crystal concentrations were formed near the upwind edge of this cloud system, and were not the product of cirrus seeding.

The convective region at A was a consistent feature of the unstable storm stages. Measurements from this region (Fig. 8) showed the convective elements to be sharply bounded and small in horizontal extent; many were as small as  $1 \text{ km}$  and yet contained liquid water contents  $> 1.0 \text{ g m}^{-3}$ . The liquid water regions were not as regularly spaced as the wave features of earlier storm stages, and liquid water contents were much higher. The convective elements were characterized by increased turbulence, positive vertical velocity, slight positive buoyancy and lower horizontal wind speeds.

The sharp edges of the convective cells were remarkable. At the upwind edge, there was one instance of a change from  $>1.0 \text{ g m}^{-3}$  to  $<0.01 \text{ g m}^{-3}$  in a distance of less than  $160 \text{ m}$ . The droplet spectrum in one of these elements, shown in Fig. 9, was broad and would have allowed the accretional growth of the ice particles.

Crystal collections from various locations on the surface were furnished to us by L. Vardiman of the Bureau of Reclamation. The surface temperature at Wolf Creek Pass on this date was about  $-10^\circ\text{C}$ . However, most of the crystals were of a type in-

<sup>5</sup> Cooper, William A. and Gabor Vali, 1976: Ice crystal concentrations in wintertime clouds. *Preprints Int. Conf. Cloud Physics*, Boulder, Amer. Meteor. Soc., 91-96.

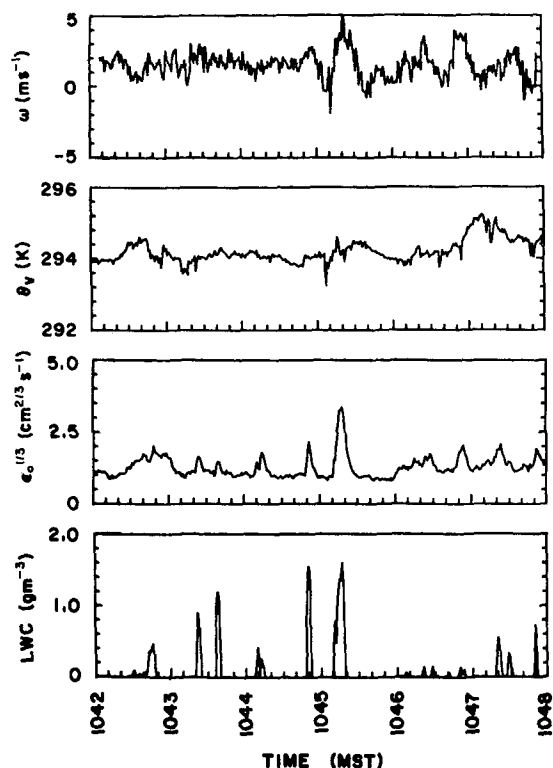


FIG. 8. Some parameters measured during flight through the convective region of the 29 December 1974 storm (B of Fig. 7). The liquid water content (LWC) is that measured by the ASSP. The value of  $\epsilon_0$  was measured by an MRI turbulence meter. The virtual potential temperature ( $\theta_v$ ) and the vertical wind ( $W$ ) are also shown.

indicating growth at colder temperatures. The crystals had the following characteristics:

(i) Most habits observed were Pla, Plc, Pld and Ple; the last three are believed to grow at  $-13^\circ\text{C}$  or

colder (Magono and Lee, 1966). The habits Plc, Pld and Ple also indicate growth near or above water saturation.

(ii) Many crystals were heavily rimed, and on at least one occasion a graupel shower was observed.

(iii) Many aggregates were collected. Some examples were found where both riming and aggregation had occurred.

(iv) The crystal collections on black felt for fixed exposure times suggested crystal concentrations of  $1-10 \text{ L}^{-1}$  for the larger crystal sizes.

These surface observations indicated that the ice crystals producing the precipitation originated  $\sim 1 \text{ km}$  above the mountain, formed in relative high concentrations (permitting aggregation), and fell through a liquid water region (permitting riming).

#### d. Dissipation storm stage

During the dissipation stage, the weakening storms broke into isolated convective cells. Precipitation was in the form of light snow showers, but did not amount to more than a trace in any of the dissipation stages. The microphysical observations showed the cells to have ice crystal concentrations similar to those in the earlier storm stages, but to have decreasing liquid water contents. The case studies showed the dissipation stage to be similar to a weak unstable stage, so no detailed case study will be presented in this paper.

## 4. Discussion of microphysical observations

### a. Supercooled water

In these studies, supercooled water was generally found in three regions. One was located over and

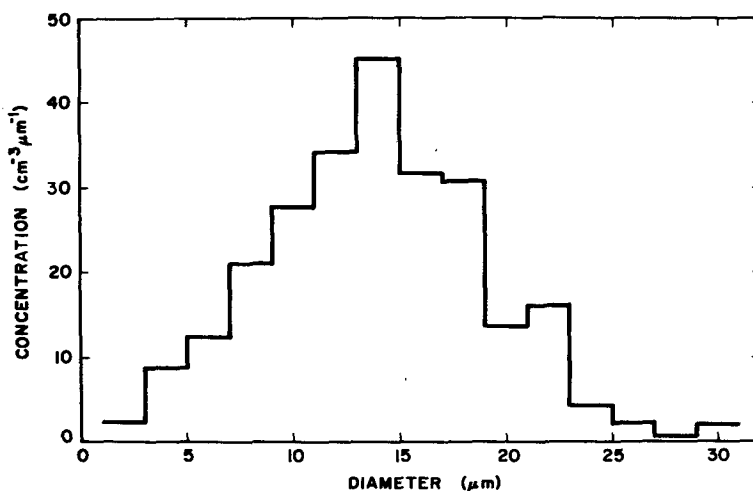


FIG. 9. An example of a broad cloud droplet spectrum detected by the ASSP in one of the convective elements penetrated near B of Fig. 7. Total droplet concentration is  $511 \text{ cm}^{-3}$ .

slightly upwind of the mountain barrier; one was located ~15–20 km upwind of the mountain and was generally associated with convection; and one was located ~60–70 km upwind of the mountains where there was an initial rise in the topography.

During stable storm stages, little liquid water was found in any of these regions. Even the region over the mountains contained liquid water contents of  $\leq 0.1 \text{ g m}^{-3}$ . This was a consequence of the blocking flow pattern at low levels, which caused the airflow at high levels to be only weakly affected by the orographic barrier. During stable storm stages, the edge of the cloud was generally more than 100 km upwind of the barrier, and there was little effect (except for some gravity wave generation) due to the upwind rise in the topography. The convective region was absent.

In the neutral storm stages the air was neutrally stratified below mountain-top altitude, and a weak horizontal convergence zone developed upwind of

the mountain. This ended the blocking flow pattern, and the resulting enhancement of the vertical air motions upwind of the mountain led to liquid water contents in the region over the mountains of typically  $0.2\text{--}0.5 \text{ g m}^{-3}$ . The convective region was still absent, but the upwind edge of the storm moved to within 60–70 km of the mountain and liquid water was present at that location.

During unstable storm stages, all three supercooled water regions were present. The water that condensed in the upwind region, however, was glaciated before it reached the vicinity of the mountains. Convection developed ~15–20 km upwind of the mountains, and this convective region apparently fed into and merged with the more extensive liquid water region over the mountains. The highest liquid water contents observed in these storms, in excess of  $1 \text{ g m}^{-3}$ , occurred over the mountains under unstable conditions.

The developing pattern in the liquid water con-

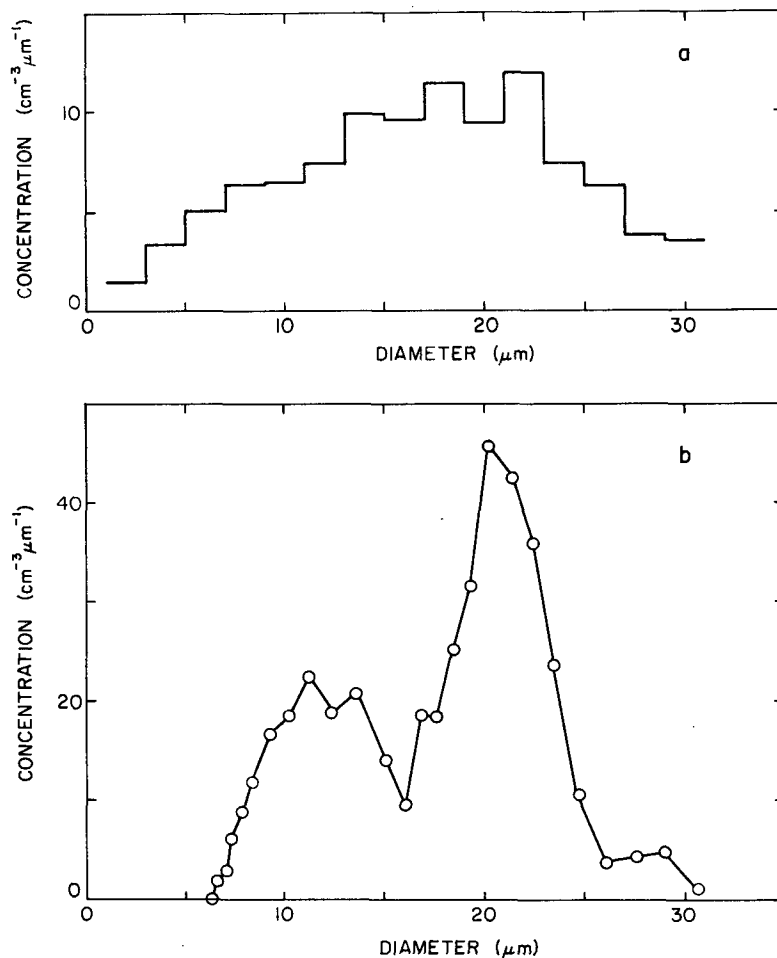


FIG. 10. Examples of the droplet spectra from over the mountains (C in Fig. 7) during an unstable storm stage. Total droplet concentration is  $210 \text{ cm}^{-3}$  in (a) and  $377 \text{ cm}^{-3}$  in (b).

tent of the region over the mountains reflected the increasing influence of the mountain on the storm as it developed from the stable to the unstable storm stage. During stable stages, the storms were generally widespread; the storm character upwind of the mountains was similar to the character over the mountains. The storms appeared to originate primarily for synoptic-scale influences. In the later unstable stages, however, the storms isolated to a greater extent on the mountains and were much more orographic in nature.

In general, the droplet spectra observed near the upwind edge of the clouds, near cloud bases, and in the lower parts of the convective elements were narrow and consisted of small droplets. However, the droplet spectra over the mountains were often composed of quite large droplets. Examples are shown in Fig. 10. The high liquid water contents and large droplets observed in region B (Fig. 7) indicate that the condensation began significantly lower, and point to an origin in the convective region A. The frequent occurrence of bimodal spectra over the mountains (e.g., Fig. 10b) may have resulted from an early rise in a convective

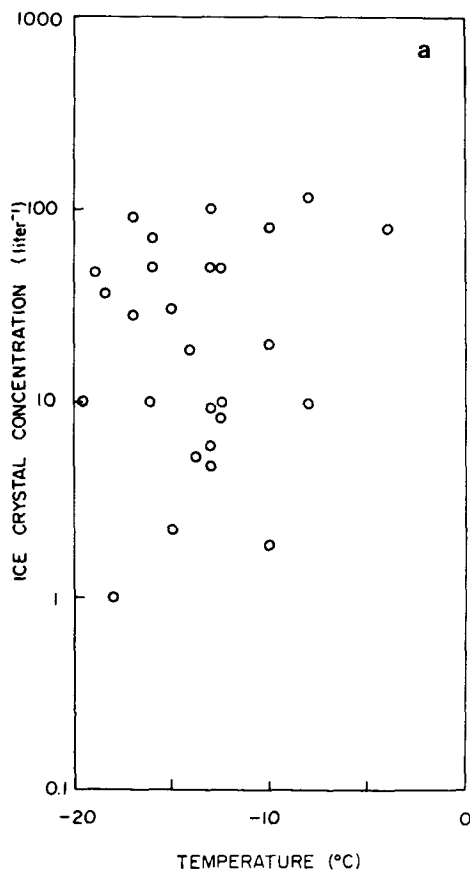


FIG. 11a. Ice crystal concentrations versus the temperature of the observation points, for all the storm traverses of these studies.

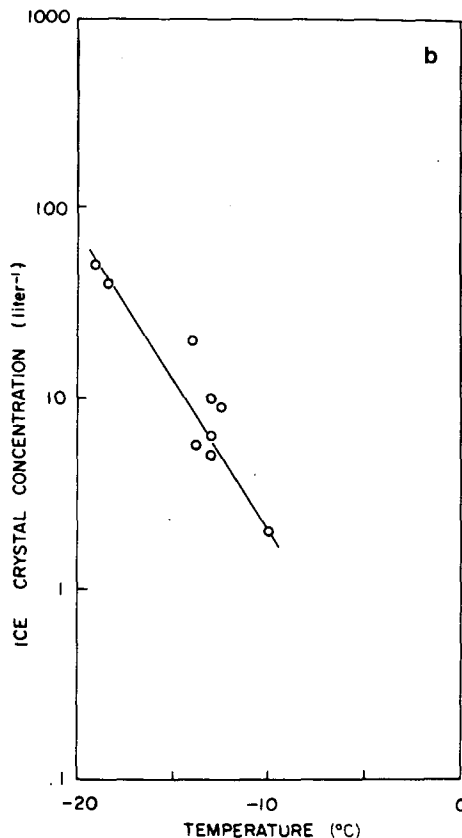


FIG. 11b. As in Fig. 11a, but including only those traverses near cloud top or where the ice crystals clearly originated at the observation temperature.

element followed by a subsequent additional rise in a stronger orographic updraft; since bimodal spectra were only observed when convection was present ahead of the mountain, their existence also supports the connection between regions A and B. The observed updraft strengths and horizontal wind speeds are also consistent with the existence of a continuous region from A to B.

#### *b. Ice crystal concentrations*

The ice crystal concentrations were surprisingly high. Concentrations above  $50 \text{ L}^{-1}$  were found in extensive regions during six of the 12 flights, and those concentrations were present in regions where they could influence the precipitation on the mountains. Concentrations this high were also found in regions that could not have been affected by seeding and where no seeding material was detected. High ice concentrations were present in all storm stages; the only exceptions were some convective elements in unstable storm stages in which concentrations  $< 1 \text{ L}^{-1}$  were found at  $-14^\circ\text{C}$ . Fig. 11a shows the range of crystal concentrations observed as a function of the temperature at the observation level.

Little correlation between ice crystal concentration and temperature is evident. The concentrations shown in this plot are quite similar to those reported by Hobbs *et al.*,<sup>6</sup> although their measurements were mostly at warmer temperatures. Much of the scatter in Fig. 11a probably results from the varied origins of the ice crystals. When cases were selected in which ice crystals were observed close to cloud edge, so that the temperature at the observation point was closely related to the temperature of formation, the points in Fig. 11b remained. There is an indication of a correlation between temperature and ice concentration in Fig. 11b, although the sample is limited.

Whenever cloud tops were lower than 6 km MSL, aircraft flights over the clouds verified that no crystals were falling into the system from higher levels. No examples of cirrus seeding of the lower layers were observed. On one occasion, crystals were observed to fall from a cirrus layer for several hundred meters but to sublimate before reaching the lower cloud layer. Even in that case, the crystal concentration falling from the cirrus layer was only about  $10 \text{ L}^{-1}$ . In most cases it was evident that concentrations of  $50\text{--}100 \text{ L}^{-1}$  could be formed in regions of the cloud warmer than  $-25^\circ\text{C}$ . A particularly clear case is 29 December 1974 in which concentrations in excess of  $50 \text{ L}^{-1}$  were formed at temperatures warmer than  $-20^\circ\text{C}$ .

Although seeding from a separate cirrus layer was not significant for these storms, the fall of crystals from higher regions of a cloud into the warm temperature regions of the same cloud was apparently an important source of high ice crystal concentrations. In many cases the crystal habits verified this fall from colder regions of the cloud.

The observed ice crystal concentrations were well above all the ice nucleus measurements obtained in these storms. Those nucleus measurements come from our own collections, the measurements of the Colorado River Basin Pilot Project and those of Hobbs *et al.*<sup>6</sup> They are as follows:

(i) Conventional Millipore samples. Filter samples were collected during these flights, each with a sample volume of  $\sim 0.2 \text{ m}^3$  per filter. These filters were processed in the Wyoming filter processor (Gordon and Vali, 1976)<sup>7</sup> at just below water saturation and at three different temperatures ( $-15$ ,  $-17$  and  $-20^\circ\text{C}$ ). Typical concentrations were  $0.01 \text{ L}^{-1}$

at  $-15^\circ\text{C}$ ,  $0.04 \text{ L}^{-1}$  at  $17^\circ\text{C}$ , and  $0.1 \text{ L}^{-1}$  at  $-20^\circ\text{C}$ . The highest nucleus concentration obtained on any filter sample from the San Juan storms was  $0.3 \text{ L}^{-1}$  at  $-20^\circ\text{C}$ .

(ii) Rotating filter samples. These samples were processed by G. Langer according to the technique of Langer and Rodgers (1975). In unseeded situations the filters only yielded  $\sim 0.1 \text{ L}^{-1}$  at  $-19^\circ\text{C}$ , and even in seeded situations the maximum concentrations indicated by these filters were  $3.0 \text{ L}^{-1}$  at  $-19^\circ\text{C}$ . Portions of these filters were collected in cloud, but other portions were clear air samples from upwind of or below the storms.

(iii) NCAR ice nucleus counter. An NCAR acoustical ice nucleus counter was operated onboard the NCAR Queen Air 304D which flew in several of these storms (as listed in Part I). Concentrations from that counter were always  $< 1 \text{ L}^{-1}$  at  $-20^\circ\text{C}$ .

(iv) Rapid expansion ice nucleus counters, operated in the target area as part of the Colorado River Basin Pilot Project. The results have been summarized by Elliott *et al.*<sup>8</sup> Typical concentrations at the surface were  $< 1 \text{ L}^{-1}$  at  $-20^\circ\text{C}$  for unseeded cases, but as high as  $50 \text{ L}^{-1}$  for seeded cases.

(v) The measurements of Hobbs *et al.*<sup>6</sup> These measurements were obtained during the year preceding our study, generally at lower levels in the storms. Under unseeded conditions the background concentrations, determined both by an NCAR counter and by Millipore filters, were  $< 0.3 \text{ L}^{-1}$ . In seeded cases concentrations  $> 100 \text{ L}^{-1}$  were detected.

The nucleus measurements do not account for the ice crystal concentrations which appeared naturally. The only ice nucleus concentrations which approached the natural concentrations were those measured at the surface and during the relatively low-level aircraft flights of Hobbs *et al.*,<sup>6</sup> and those were apparently due to seeding. Either a nucleation process different from those measured by the above techniques is responsible for the production of the natural ice or an ice multiplication mechanism must be active.

The evidence did not favor ice multiplication. Ice concentrations normally increased rapidly near cloud edge, then stabilized deeper into the storm systems. In particular, the mechanism suggested by Hallett and Mossop (1974) was not important, because the high ice concentrations originated at temperatures much colder than  $-8^\circ\text{C}$ . (When high ice concentrations were detected at temperatures warmer than  $-8^\circ\text{C}$ , the habits of the crystals indicated an origin at colder temperatures.) In cases where rapid increases in ice concentration were

<sup>6</sup> Hobbs, P. V., L. F. Radke, J. R. Fleming and D. G. Atkinson, 1975: Airborne ice nucleus and cloud microstructure measurements in natural and artificially seeded situations over the San Juan Mountains of Colorado. Research Rep. X, Contributions from the Cloud Physics Group, University of Washington, 89 pp.

<sup>7</sup> Gordon, G., and G. Vali, 1976: University of Wyoming thermal diffusion chamber. *Proc. Third Int. Workshop Ice Nucleus Measurements*, Laramie, National Science Foundation, 91-122.

<sup>8</sup> Elliott, Robert D., R. W. Shaffer, A. Court and J. F. Hanneford, 1976: Colorado River Basin Pilot Project Comprehensive Evaluation Report. Aerometric Research Inc. Rep. ARI-76-1 to the U.S. Bureau of Reclamation. [NTIS PB-262 057/3ST].

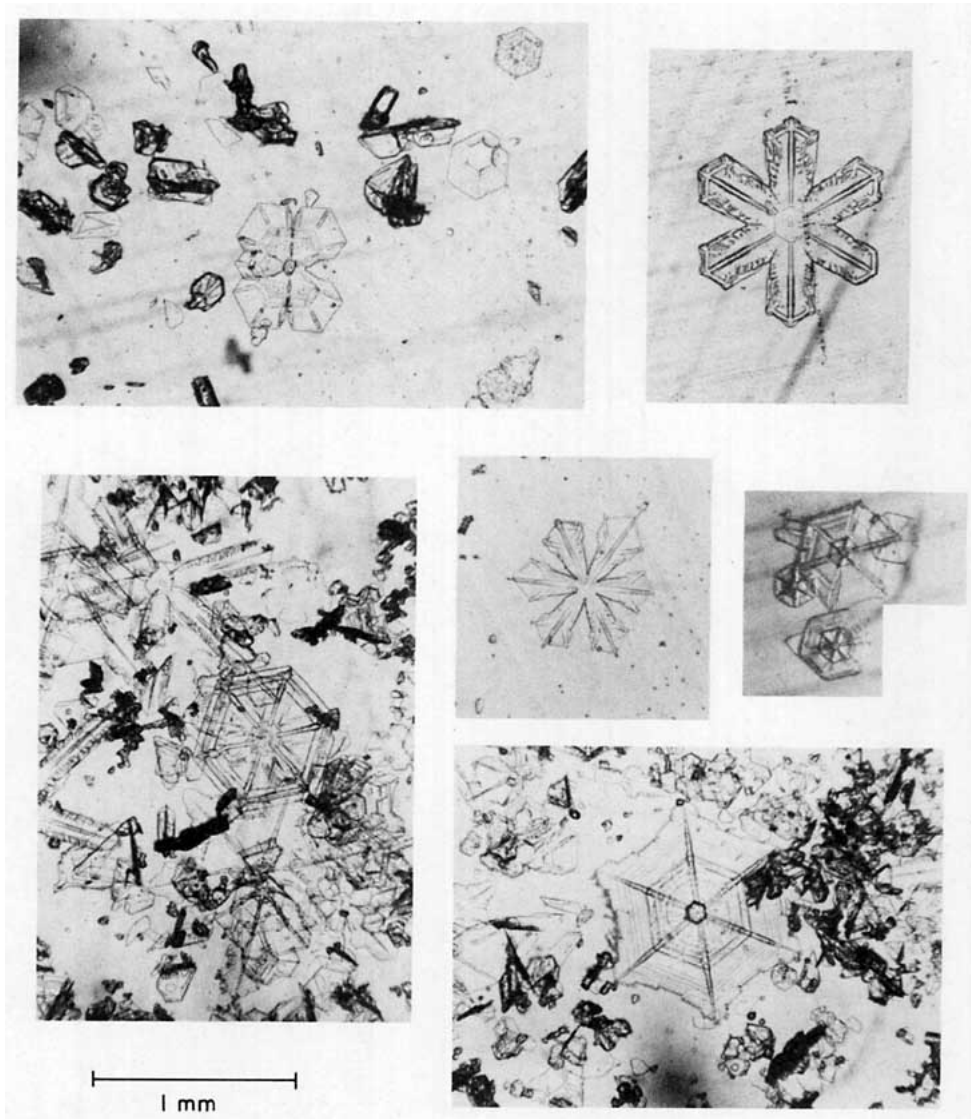


FIG. 12. Examples of ice crystals collected on decelerator slides during early, stable stages of storms.

seen (such as at the upwind edge of the storm shown in Fig. 7), the cloud droplet spectrum was narrow and not suitable for the mechanism of Hallett and Mossop. The observed ice development was also not consistent with that expected from the multiplication mechanisms of Hobbs and Alkezweeny (1968), Hobbs and Farber (1972) or Vardiman and Grant (1974).<sup>9</sup>

### c. Precipitation mechanisms

During stable storm stages, ice crystals collected from the aircraft and at the surface were mostly

unrimed or lightly rimed. Some examples from a stable storm stage are shown in Fig. 12. The low degree of riming was consistent with the low liquid water contents detected during this storm stage. The absence of rime on the surface collections further supports the absence of any significant supercooled water in the regions too close to the mountains for aircraft penetrations. The dominant precipitation formation mechanism during the stable storm stage was diffusional growth of ice crystals to sizes which could fall against the weak updrafts of that stage.

During neutral storm stages, unrimed or lightly rimed crystals were often observed far upwind of the mountains. In regions close to the mountains, the crystals showed evidence of both accretional growth and aggregation. Most of the precipita-

<sup>9</sup> Vardiman, L., and L. O. Grant, 1974: The generation of secondary ice particles in clouds by crystal-crystal collisions. *Preprints Conf. Cloud Physics*, Tucson, Amer. Meteor. Soc.

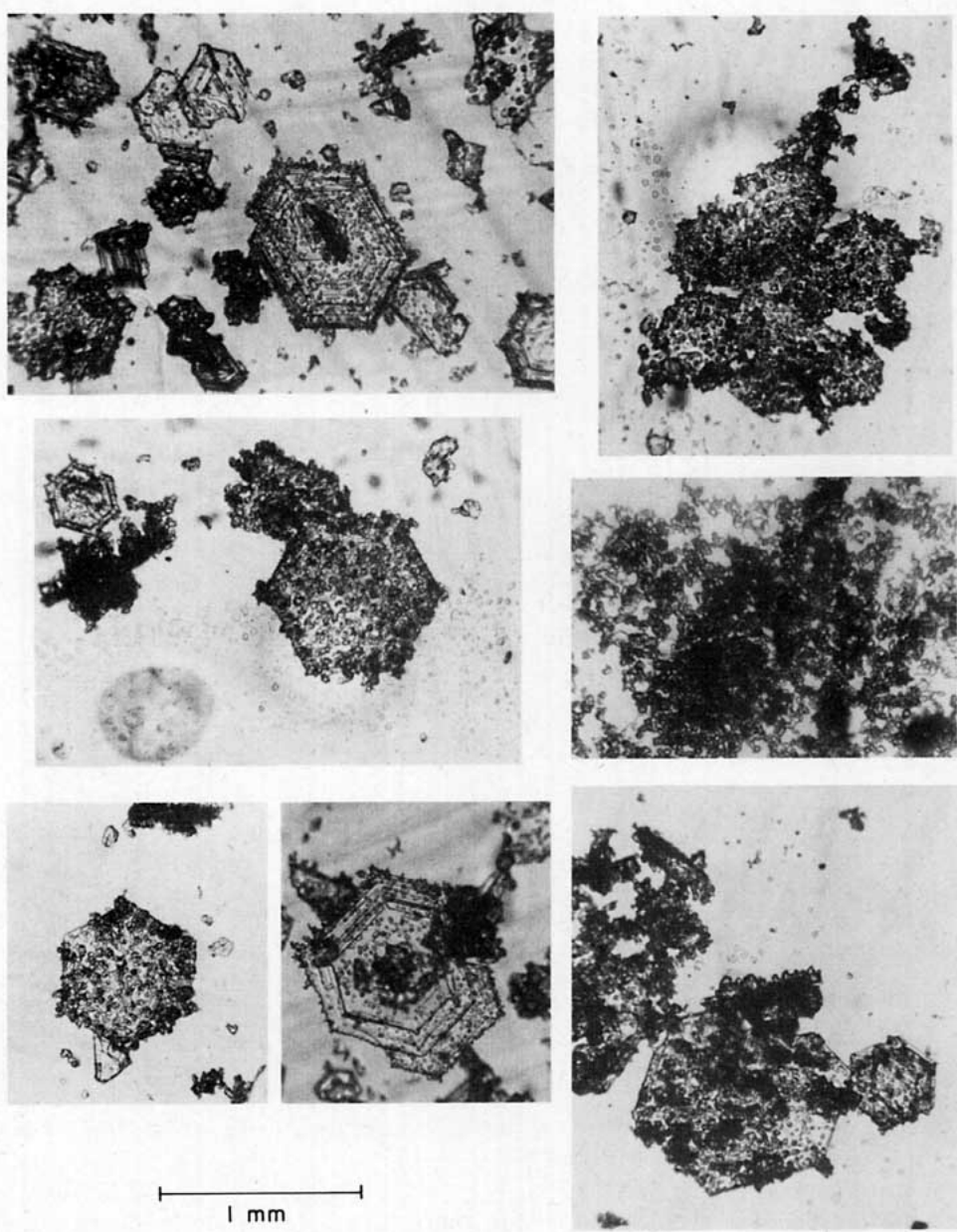


FIG. 13. Examples of ice crystals collected on decelerator slides during later, unstable stages of storms.

tion collected at the surface showed significant riming during this storm stage, but most crystal habits were still recognizable. It appeared that most of the mass in the precipitation was still due to vapor growth.

In the unstable storm stage, the crystals were generally heavily rimed. Examples of the decelerator collections are shown in Fig. 13. Occasionally graupel showers were observed at the surface, and the precipitation collected at the surface was so heavily rimed that the vapor-grown crystals were often unrecognizable. Accretional growth of the precipitation was clearly important and was probably dominant during the unstable storm stage.

The precipitation records often showed two maxima, one in the stable storm stage and one in the unstable stage. The first maximum was apparently due to the high cloud tops which gave a maximum depth to the storm in the stable storm stage. The second maximum occurred when convection provided liquid water regions and made accretional growth possible.

## 5. Conclusions

Aircraft observations of the microphysical nature of San Juan wintertime storms have shown that these storms contained surprisingly high ice crystal con-

centration and relatively low liquid water contents. Furthermore, those liquid water regions were generally restricted in extent. The initial storm stage, the stable stage, generally had the lowest supercooled water contents, and the unstable storm stage had the highest water contents. The dominant precipitation process in these storms was a vapor growth process during most storm periods, but the accretional growth process was at least equally important in the unstable storm stages. The nature of the storms evolved from an initial large-scale storm to a storm whose character was predominantly orographic.

Ice crystal concentrations of  $10\text{--}100\text{ L}^{-1}$  were found in most of the precipitating storms, even when cloud top temperatures were near  $-20^{\circ}\text{C}$  or warmer. These ice crystal concentrations were about two orders of magnitude above all corresponding ice nucleus measurements. The ice concentrations could not be attributed to known ice multiplication mechanisms.

*Acknowledgments.* The participation of Dr. Vardmann in the operations was particularly important to their success, and the ice crystal collections which he supplied were valuable supplements to our data. Other CRBPP participants, notably Western Scientific Services, Inc., and EG&G, were very helpful in supplying supporting data. G. Langer loaned us a rotating filter sampler and processed the filters, and Patricia Walsh helped analyze the cloud droplet data. Acknowledgment is also made to

the National Center for Atmospheric Research, which is sponsored by the National Science Foundation, for computer time used in the analysis of the aircraft data. Particular thanks are due to Dr. D. L. Veal and George Chamberlin for conducting the aircraft operations and for their many additional contributions to this research.

#### REFERENCES

- Cooper, William A., and John D. Marwitz, 1980: Winter storms over the San Juan Mountains. Part III: Seeding potential. *J. Appl. Meteor.*, **19**, 100–107.
- Dye, J. E., G. Langer, V. Toutenhoofd, T. W. Cannon and C. A. Knight, 1976: Use of a sailplane to measure microphysical effects of silver iodide seeding in cumulus clouds. *J. Appl. Meteor.*, **15**, 264–274.
- Hallett, J., and S. Mossop, 1974: Production of secondary ice particles during the riming process. *Nature*, **249**, 26–28.
- , and A. J. Alkezweeny, 1968: The fragmentation of freezing water droplets in free fall. *J. Atmos. Sci.*, **25**, 881–888.
- , and R. J. Farber, 1972: Fragmentation of ice particles in clouds. *J. Rech. Atmos.*, **6**, 245–258.
- Langer, G., and J. Rodgers, 1975: An experimental study of the detection of ice nuclei on membrane filters and other substrata. *J. Appl. Meteor.*, **14**, 560–570.
- Magono, C., and C. W. Lee, 1966: Meteorological classification of natural snow crystals. *J. Fac. Sci. Hokkaido Univ.*, Ser. VII, **2**, 321–326.
- Marwitz, John D., 1980: Winter storms over the San Juan Mountains. Part I: Dynamic processes. *J. Appl. Meteor.*, **19**, 913–926.
- Turner, E. M., and L. F. Radke, 1973: The design and evaluation of an airborne optical ice particle counter. *J. Appl. Meteor.*, **12**, 1309–1318.
- , and P. V. Hobbs, 1976: Optical techniques for counting ice particles in mixed-phase clouds. *Atmos. Tech.* (NCAR), No. 8, Spring 1976, 25–31.